Two-photon photoassociation spectroscopy of CsYb: Ground-state interaction potential and interspecies scattering lengths

A. Guttridge,[1] Matthew D. Frye,[2] B. C. Yang,[2] Jeremy M. Hutson,[2,*] and Simon L. Cornish[1,†]

[1]*Joint Quantum Centre (JQC) Durham-Newcastle, Department of Physics, Durham University, South Road, Durham DH1 3LE, United Kingdom*

[2]*Joint Quantum Centre (JQC) Durham-Newcastle, Department of Chemistry, Durham University, South Road, Durham DH1 3LE, United Kingdom*

(Received 1 June 2018; published 31 August 2018)

We perform two-photon photoassociation spectroscopy of the heteronuclear CsYb molecule to measure the binding energies of near-threshold vibrational levels of the $X\,^2\Sigma^+_{1/2}$ molecular ground state. We report results for ^{133}Cs^{170}Yb, ^{133}Cs^{173}Yb, and ^{133}Cs^{174}Yb, in each case determining the energy of several vibrational levels including the least-bound state. We fit an interaction potential based on electronic structure calculations to the binding energies for all three isotopologs and find that the ground-state potential supports 77 vibrational levels. We use the fitted potential to predict the interspecies s-wave scattering lengths for all seven Cs+Yb isotopic mixtures.

DOI: 10.1103/PhysRevA.98.022707

I. INTRODUCTION

Mixtures of ultracold atomic gases provide an appealing platform for numerous avenues of research, including the investigation of novel quantum phases [1–7], the study of Efimov physics [8–11], and the creation of ultracold polar molecules [12–22]. Early experiments explored bi-alkali-metal gases [23–33], but there is currently a growing interest in mixtures composed of alkali-metal and closed-shell atoms [34–41]. Such mixtures open up the possibility of creating paramagnetic ground-state polar molecules, with applications in quantum simulation and quantum information [42–44], precision measurement [45], tests of fundamental physics [46–48], and tuning of collisions and chemical reactions [49,50]. In pursuit of this goal, we have constructed an apparatus to investigate ultracold mixtures of Cs and Yb [51–53].

Magnetoassociation on a Feshbach resonance has proved a highly successful technique for producing weakly bound ultracold molecules [12,54]. When combined with optical transfer using stimulated Raman adiabatic passage (STIRAP), the approach has allowed the production of a range of ultracold polar bi-alkali molecules in the rovibrational ground state [13,17,19–21]. Unfortunately, in the case of an alkali-metal atom and a closed-shell atom, the Feshbach resonances are predicted to be narrow and sparsely distributed in magnetic field [55,56]. Nevertheless, such resonances have recently been observed experimentally in the RbSr system [57], though magnetoassociation remains unexplored. The resonances in CsYb are predicted to be particularly favorable for magnetoassociation [58]. However, to predict their locations accurately, it is necessary first to determine the binding energies of the near-threshold vibrational levels of the CsYb molecule.

In this paper, we present two-photon photoassociation spectroscopy of the heteronuclear CsYb molecule. Using ultracold mixtures of Cs and Yb confined in an optical dipole trap, we accurately measure the binding energies of the near-threshold vibrational levels of CsYb molecules in the $X\,^2\Sigma^+_{1/2}$ ground state. We report results for three isotopologs, ^{133}Cs^{170}Yb, ^{133}Cs^{173}Yb, and ^{133}Cs^{174}Yb, in each case measuring the energy of several vibrational levels including the least-bound state. We fit an interaction potential based on electronic structure calculations to the binding energies for all three isotopologs and find that the ground-state potential supports 77 vibrational levels. The excellent agreement between our model and the experimental results allows us to calculate the interspecies scattering lengths for ^{133}Cs interacting with all seven stable Yb isotopes.

II. TWO-PHOTON PHOTOASSOCIATION SPECTROSCOPY

A. Overview

The two-photon photoassociation process is shown in Fig. 1. This scheme is an extension of one-photon photoassociation [60,61], whereby a pair of colliding atoms is associated to form a molecule in a rovibrational level of an electronically excited molecular state. The laser that drives the one-photon photoassociation, L_1, has frequency ω_1 and intensity I_1; it is detuned from a free-bound transition by Δ_{FB}. The second laser L_2 has frequency ω_2 and intensity I_2; it couples the electronically excited molecule to a rovibrational level of the molecule in the electronic ground state. Its detuning from this bound-bound transition is Δ_{BB}. When L_2 is resonant with a bound-bound transition, the coupling leads to the formation of a dark state and the suppression of the absorption of L_1. Such two-photon dark resonances can be used to measure the binding energies E_{b1} of vibrational levels of the molecule in

*j.m.hutson@durham.ac.uk
†s.l.cornish@durham.ac.uk

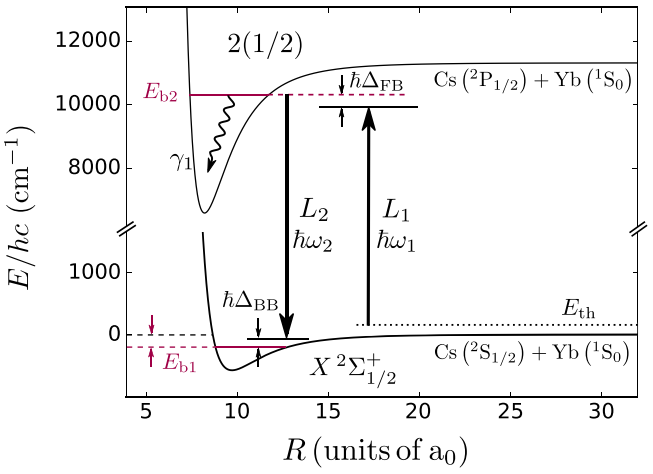

FIG. 1. Two-photon photoassociation for the measurement of the binding energy, E_{b1}, of a vibrational level of CsYb in its electronic ground state. A pair of colliding Cs and Yb atoms with thermal energy E_{th} is associated to form a CsYb molecule in a rovibrational level of the electronically excited 2(1/2) state by light of frequency ω_1. This rovibrational level is coupled to a level in the electronic ground state, $X\,^2\Sigma^+_{1/2}$, by light of frequency ω_2. The molecular curves plotted here are adapted from Ref. [59]. The internuclear distances where the transitions occur are not shown to scale.

the electronic ground state. In the undressed, zero-temperature limit, the binding energy is given simply by the difference in photon energy of the two lasers, $E_{b1} = \hbar(\omega_2 - \omega_1)$, when on two-photon resonance. This technique has been applied in a large number of single-species [62–71] and two-species ultracold atom experiments [13,72–76] with considerable success.

For the specific case of CsYb discussed in this paper, the first photon excites the colliding atoms into a rovibrational level of the molecule close to the Cs($^2P_{1/2}$) + Yb($^1S_0$) asymptote. The electronic state at this threshold is designated 2(1/2) to indicate that it is the second (first-excited) state with total electronic angular momentum $\Omega = 1/2$ about the internuclear axis. It correlates at short range with the $1\,^2\Pi_{1/2}$ electronic state in Hund's case (a) notation [59], but at long range the $1\,^2\Pi_{1/2}$ and $2\,^2\Sigma_{1/2}$ states are strongly mixed by spin-orbit coupling. We have recently reported photoassociation spectroscopy of the vibrational levels of the molecule within 500 GHz of the 2(1/2) threshold [77]. In this work, we add a second photon to couple the vibrational level in the electronically excited state to a near-threshold level of the $X\,^2\Sigma^+_{1/2}$ electronic ground state. We label each vibrational level by its vibrational number n below the associated threshold, such that $n = -1$ corresponds to the least-bound state, using n' for the electronically excited state and n'' for the ground state. Because of the low temperature of our atomic mixtures, combined with the selection rule $\Delta N = 0$, all the rovibrational levels we measure have rotational quantum number $N = 0$.

B. Experimental setup

The experimental setup has been described in the context of our previous work [39,51–53,77]. Here we focus on details of the ultracold atomic mixtures and the two-photon photoassociation setup.

Our measurements are performed on mixtures of Cs and Yb confined in an optical dipole trap (ODT). The ODT is formed from the output of a broadband fiber laser (IPG YLR-100-LP) with a wavelength of 1070(3) nm and consists of two beams crossed at an angle of 40° with waists of 33(4) μm and 72(4) μm. The measured Yb (Cs) trap frequencies are 240 (750) Hz radially and 40 (120) Hz axially. The trap depths for the two species are $U_{Yb} = 5\ \mu$K and $U_{Cs} = 85\ \mu$K, respectively. We load the ODT with a mixture of 7×10^4 Cs atoms at $T_{Cs} = 6\ \mu$K in the absolute ground state $6\,^2S_{1/2}\,|F = 3, m_F = +3\rangle$ and Yb atoms at $T_{Yb} = 1\ \mu$K in the $^1S_0$ ground state. The number of Yb atoms depends on the Yb isotope involved. Typically, we use 8×10^5 atoms for ^{174}Yb, 4×10^5 atoms for ^{170}Yb, or 3×10^5 atoms for ^{173}Yb. For both atomic species, the atom number is measured using resonant absorption imaging after a short time of flight.

The light for two-photon photoassociation is derived from two independent lasers. L_1 is a Ti:sapphire laser (M Squared SolsTiS) and L_2 is a distributed Bragg reflector (DBR) laser. Both lasers are frequency stabilized using a high-finesse optical cavity, the length of which is stabilized to a Cs atomic transition using the Pound-Drever-Hall method [78]. The light sent to the optical cavity from L_1 and L_2 is first passed through two independent broadband-fiber electro-optic modulators (EOMs) (EOSPACE PM-0S5-10-PFA-PFA-895) to add frequency sidebands. We then utilize the "electronic sideband" technique [79,80] to allow continuous tuning of the two laser frequencies; by stabilizing a frequency sideband to a cavity transmission peak, the carrier frequencies of both lasers may be tuned over the 748.852(5) MHz free spectral range (FSR) of the cavity by changing the modulation frequencies applied to the EOMs. By stabilizing the two lasers to different modes of the cavity, we can control their frequency difference, $\omega_1 - \omega_2$, over many GHz.

The main outputs of lasers L_1 and L_2 are overlapped, transmitted through an acousto-optic modulator (AOM) for fast intensity control and coupled into a fiber that carries the light to the experiment. The output of the fiber is focused onto the atomic mixture with a waist of 150 μm and is circularly polarized to drive σ^+ transitions. This polarization gives us the strongest two-photon transitions from the Cs($6\,^2S_{1/2}F = 3, m_F = +3$) + Yb($^1S_0$) scattering state to the $F = 3$ manifold of the molecular electronic ground state via an intermediate vibrational level of CsYb in the $F' = 4$ manifold of the 2(1/2) excited state [77].

We measure the frequency difference between lasers L_1 and L_2 using one of three methods, depending on the binding energy of the state under investigation. Most generally, the frequency difference is determined from the difference in the modulation frequencies applied to the two EOMs, combined with the number of cavity FSRs between the two modes used for frequency stabilization. Light from both lasers is coupled into a commercial wavemeter (Bristol 671A) for absolute frequency calibration and unambiguous determination of the cavity mode. For binding energies below 2 GHz, the frequency difference between the two lasers is measured directly from the beat frequency recorded on a fast photodiode (EOT ET-2030A). In the special case of the least-bound state, we do not use a DBR laser and instead we drive the AOM with two rf frequencies. Generating the two-photon detuning in this way

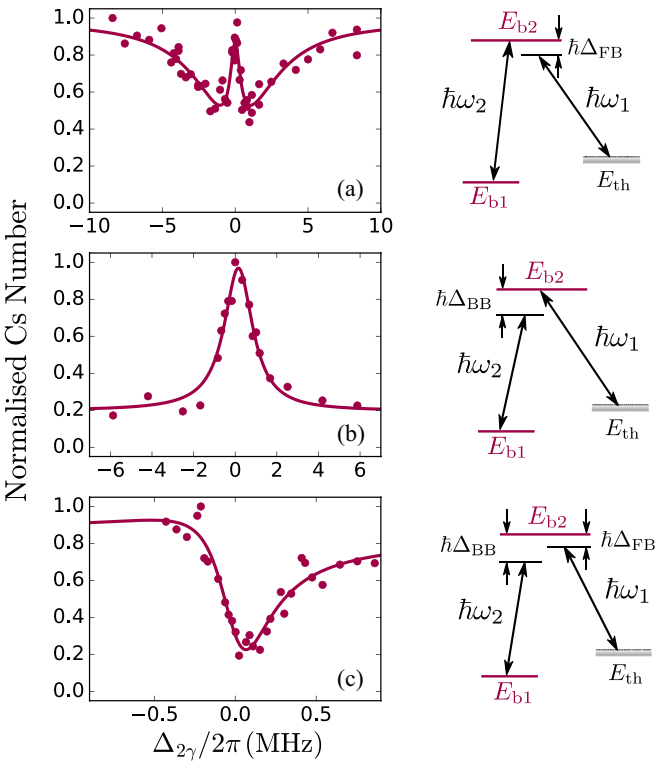

FIG. 2. Measurement of the least-bound state of $Cs^{174}Yb$ in the $X\,^2\Sigma^+_{1/2}$ electronic ground state by two-photon photoassociation spectroscopy. The intermediate state used is the $n' = -13$ level of the molecule in the 2(1/2) state. Left panels: Two-photon photoassociation spectra. Normalized number of Cs atoms plotted against $\Delta_{2\gamma} = \Delta_{FB} - \Delta_{BB}$. Right panels: Simplified level structure for the two-photon photoassociation transitions. (a) Dark-resonance spectroscopy performed by scanning ω_1. The red solid line shows a fit using Eq. (1), the analytical solution of the optical Bloch equations for a λ-type three-level system. The best-fit parameters are $\Omega_{BB}/2\pi = 2(1)$ MHz, $\Gamma/2\pi = 6(1)$ MHz, and $\Gamma_{eff}/2\pi = 2(1) \times 10^2$ kHz. (b) Dark-resonance spectroscopy performed by scanning ω_2. The red solid line shows a fit using a Lorentzian profile. (c) Raman spectroscopy. The red solid line shows a fit using a Fano profile. The spectra shown in (a)–(c) were obtained with laser intensities $I_1 = 0.42, 0.68, 1.1$ W/cm^2 and $I_2 = 0.79, 0.57, 0.76$ W/cm^2, respectively.

eliminates any effects of laser frequency noise and allows a very precise determination of the frequency difference.

C. Experimental results

Two-photon photoassociation measurements are performed by illuminating the atomic mixture with light from lasers L_1 and L_2 for a variable time up to 250 ms, in a magnetic field of 2.2(2) G. Figure 2 shows the two-photon feature for the least-bound $n'' = -1$ level of $Cs^{174}Yb$, using the $n' = -13$ level of the 2(1/2) state as the intermediate state. We detect the two-photon resonance by measuring the number of Cs atoms remaining after exposure to the photoassociation light as a function of the two-photon detuning $\Delta_{2\gamma} = \Delta_{FB} - \Delta_{BB}$. Three different line shapes may be observed, depending on the relative intensities and detunings of the lasers.

Figure 2(a) shows the line shape observed using two-photon dark-resonance spectroscopy [73,81]. In this method, ω_2 is fixed on resonance with the bound-bound transition ($\Delta_{BB} = 0$) and ω_1 is scanned over the free-bound transition. The spectrum exhibits the w-shaped profile expected for electromagnetically induced transparency (EIT) in a λ-type three-level system [82] and we therefore refer to this as the EIT line shape. In the wings, we observe a Lorentzian profile originating from one-photon photoassociation to the $n' = -13$ level of the 2(1/2) state. Then, on resonance, we see a suppression of the photoassociative loss due to the creation of a dark state composed of the initial atomic scattering state and the molecular ground state. This dark state is decoupled from the intermediate $n' = -13$ state and leads to the observed "transparency." We fit the data with the analytical solution of the optical Bloch equations for a λ-type three-level system [73,82] in the limit of $\Omega_{FB} \ll \Omega_{BB}$,

$$\frac{N}{N_0} = \exp\left\{-\frac{t_{PA}\Omega_{FB}^2\left[4\Gamma\Delta_{2\gamma}^2 + \Gamma_{eff}\left(\Omega_{BB}^2 + \Gamma_{eff}\Gamma\right)\right]}{\left|\Omega_{BB}^2 + (\Gamma + 2i\,\Delta_{FB})(\Gamma_{eff} + 2i\,\Delta_{2\gamma})\right|^2}\right\}. \quad (1)$$

Here, t_{PA} is the irradiation time of the photoassociation lasers, Ω_{FB} (Ω_{BB}) is the Rabi frequency on the free-bound (bound-bound) transition, $\Delta_{2\gamma}$ is the detuning from two-photon resonance, Γ is the power-broadened linewidth of the free-bound transition, and Γ_{eff} is a phenomenological constant that accounts for the decoherence of the dark state.

Figure 2(b) shows the dark-resonance spectrum observed when ω_1 is resonant with the free-bound transition ($\Delta_{FB} = 0$) and ω_2 is scanned. This complements the EIT line shape shown in Fig. 2(a); the only difference is which laser frequency is scanned. Off resonance with the bound-bound transition, we observe a large loss of Cs atoms due to the production of Cs*Yb molecules [83]. When L_2 is tuned close to resonance with the bound-bound transition, the photon-dressed ground state and the excited state couple to form two dressed states [82]. The splitting of the dressed states creates a dark state where L_1 is no longer resonant with the free-bound transition. Therefore, the production of Cs*Yb molecules is suppressed and there is a recovery in the Cs number. In the perturbative limit, Eq. (1) reduces to a Lorentzian profile with a width proportional to Ω_{BB}^2 and we therefore fit the data with a Lorentzian line shape. This dark-resonance technique is the simplest method for the observation of a two-photon resonance, as with sufficient L_2 intensity the feature can be significantly broadened without shifting the line center. However, the background number of Cs atoms is sensitive to the one-photon photoassociation loss rate and can therefore drift in response to changes in the Yb density, the Cs density, or the photoassociation light intensity or polarization.

Figure 2(c) shows an alternative method for observing the two-photon resonance using Raman spectroscopy. In this case, ω_1 is detuned from the free-bound transition ($\Delta_{FB} = -15$ MHz) and L_2 drives a stimulated Raman transition to a vibrational level of the electronic ground state when the Raman condition is fulfilled ($\Delta_{FB} = \Delta_{BB}$). This gives a narrow line shape. The creation of a ground-state CsYb molecule, which is dark to our imaging, causes a decrease in the number of observed Cs atoms. The asymmetric line shape originates from the interference between the two paths ($E_{th} \rightarrow E_{b_2}$ and $E_{th} \rightarrow E_{b_2} \rightarrow E_{b_1} \rightarrow E_{b_2}$) [84,85] and incorporates a Fano profile [86].

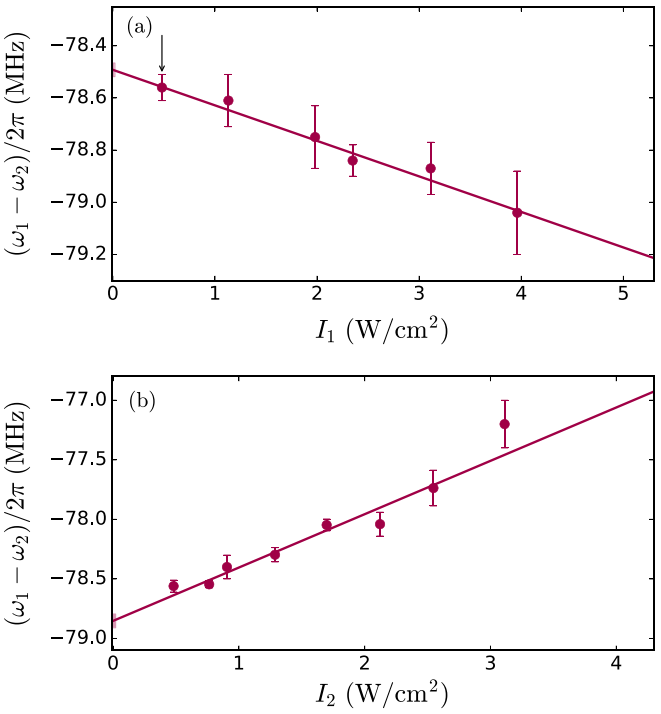

FIG. 3. Light shift of the $Cs^{174}Yb$ $n''=-1$ Raman line as a function of photoassociation laser intensity, using the $n'=-13$ intermediate state. (a) Measured line-center frequency as a function of intensity I_1 of laser L_1 driving the free-bound transition. The intensity of laser L_2 for this data set was $I_2=0.35$ W/cm^2. (b) Measured line-center frequency as a function of intensity I_2 of laser L_2 driving the bound-bound transition. The intensity of laser L_1 for this data set was $I_1=0.48$ W/cm^2 and is highlighted in (a). The 1σ uncertainties in the intercepts are represented by the shaded regions at the origins.

We use Raman spectroscopy as the primary method for the observation of $n''=-1$ levels, as the line shape of the two-photon feature is narrow for low powers of L_1 and L_2. However, coupling of the ground and excited states by L_1 and L_2 causes light shifts in both levels that are linear in laser intensity in the perturbative limit [85]. Figure 3 shows the shifts $\delta_1(I_1)$ and $\delta_2(I_2)$ of the two-photon resonance position as functions of the intensities of lasers L_1 and L_2. We fit a straight line to the data to extract the line position at zero intensity. As expected, the gradient of the shift with respect to intensity is larger for the bound-bound transition, due to the larger Franck-Condon factor (FCF) between two bound states than between a bound state and a scattering state.

Further systematic effects that may shift the position of the Raman line are the ac Stark shift due to the dipole trapping light, the Zeeman effect due to the magnetic field, and the finite energy of the initial atomic collision. The trapping light may systematically shift the line position by a differential ac Stark shift between the atomic pair and the molecular state E_{b1}. However, this shift is expected to be small for the weakly bound states considered here. The effect of magnetic field on the results is small, as the linear Zeeman shift is almost the same for the atomic state and the molecular state. Investigation of the shifts due to both magnetic field and dipole trap intensity found no significant shift at the resolution of the measurements

TABLE I. Observed binding energies and their uncertainties for vibrational levels of three different isotopologs of CsYb in its electronic ground state, together with experimental 1σ uncertainties and binding energies calculated from the fitted interaction potential.

Yb			E_{b1}/h (MHz)			
isotope	n'	n''	Observed	Uncertainty	Calculated	Obs. − Calc.
170	−15	−1	15.7	0.3	15.6	0.1
170	−15	−3	1576	2	1576	0
170	−15	−4	4259	2	4257	2
170	−15	−5	8988	2	8989	1
173	−13	−1	56.8	0.2	57.0	0.2
173	−13	−2	592	1	591	1
173	−13	−3	2166	1	2165	1
174	−13	−1	78.66	0.09	78.73	0.07
174	−17	−1	78.7	0.1	78.7	0.0
174	−17	−2	686.4	0.7	686.5	0.1
174	−17	−3	2385.5	0.9	2384.5	1
174	−17	−4	5749	1	5747	2
174	−17	−5	11358	1	11359	1
174	−17	−6	19803	1	19805	2
174	−17	−7	31672	2	31668	4

(<100 kHz). The remaining systematic shift is the thermal shift E_{th} due to the energy of the initial collision between the Cs and Yb atoms. We account for this by subtracting the mean collision energy $E_{th}=\frac{3}{2}\mu k_B(T_{Yb}/m_{Yb}+T_{Cs}/m_{Cs})$, where μ is the reduced mass. For our initial temperatures of $T_{Yb}=1\,\mu$K and $T_{Cs}=6\,\mu$K, the correction is of the order of 100 kHz and is insignificant except for the measurements of the $n''=-1$ levels.

In total, we observed 14 ground-state vibrational levels for the three isotopologs $Cs^{170}Yb$, $Cs^{173}Yb$, and $Cs^{174}Yb$. The binding energies of these levels, corrected for thermal shifts and light shifts due to L_1 and L_2, are listed in Table I. The dark-resonance spectroscopy method scanning ω_2 was used for measurements of the $n''<-1$ levels. The smaller error bars for the $n''=-1$ levels result from the narrower Raman feature and the different method of generating the small frequency offset between the two photons. Frequency instabilities due to beating between the sidebands of L_1 and L_2 prevented observation of the $n''=-2$ state of $Cs^{170}Yb$. The $n''=-1$ level of $Cs^{174}Yb$ was measured with both $n'=-13$ and $n'=-17$ as intermediate states to verify that the measurements are of the ground electronic state and not two-photon transitions to a higher-energy electronic state. We chose to use intermediate states with moderately large binding energies to increase the detuning of the photoassociation light from the Cs D_1 transition; a greater feature depth is observed for larger detuning due to the reduction of off-resonant Cs losses [77].

III. LINE STRENGTHS AND AUTLER-TOWNES SPECTROSCOPY

The strengths of transitions between the electronically excited state and ground state may be determined from the light shift of the Raman spectroscopy measurements. The systematic dependencies of Raman transitions in three-level

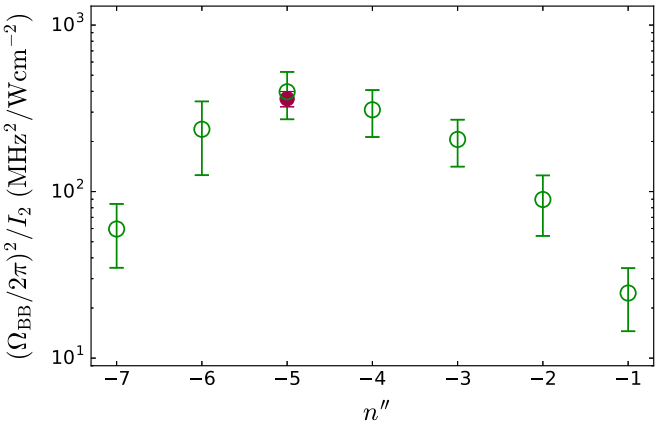

FIG. 4. Measured line strengths of $n' = -17 \rightarrow n''$ transitions in $Cs^{174}Yb$. The line strength Ω_{BB}^2/I_2 is plotted as a function of ground-state vibrational level n''. Green open circles represent measurements of the Rabi frequencies from the line shifts of the Raman loss features. The filled red circle represents the measurement of the $n' = -17 \rightarrow n'' = -5$ transition using Autler-Townes spectroscopy.

λ-type systems have been studied extensively [84,87–90]. For atomic systems, it has been shown that the light shift is proportional to Ω^2, where Ω is the Rabi frequency associated with either one-photon transition [87,88]. Investigations of molecular systems have found that the light shift of the resonance maintains this Ω^2 dependence even in the presence of decay out of the three-level system [85,91]. Here we determine the line strengths for the bound-bound transitions given by Ω_{BB}^2/I_2 using light-shift measurements of the type presented in Fig. 3(b).

For the Raman line shape shown in Fig. 2(c), the maximum loss of Cs atoms occurs at a two-photon detuning $\omega_1 - \omega_2 = E_{b1}/\hbar + \delta_1(I_1) + \delta_2(I_2)$. Here, $\delta_1(I_1)$ and $\delta_2(I_2)$ are the light shifts of the transition and [85]

$$\frac{\delta_2(I_2)}{I_2} = \left(\frac{\Omega_{BB}^2/I_2}{4\Delta_{FB}^2 + \Gamma^2}\right)\Delta_{FB}, \tag{2}$$

where $\Delta_{FB} \simeq \Delta_{BB}$ in the vicinity of the Raman resonance [92]. It follows that the line strength Ω_{BB}^2/I_2 may be obtained from the gradient of resonance position with respect to intensity I_2 using Eq. (2). The results for the measured line strengths of $n' = -17 \rightarrow n''$ transitions in $Cs^{174}Yb$ are presented in Fig. 4 as green open circles.

The line strengths of the bound-bound transitions may also be determined using Autler-Townes spectroscopy (ATS) to measure the Rabi frequency, Ω_{BB}, directly from the splitting of the two dressed states. The experimental configuration for ATS is the same as in Fig. 2(a), but instead of measuring the binding energy we measure the splitting of the dressed states as a function of the intensity of L_2. Figure 5 shows the Autler-Townes spectrum of the $n' = -17 \rightarrow n'' = -5$ transition in $Cs^{174}Yb$. In the figure, ω_2 is fixed on resonance ($\Delta_{BB} = 0$) and ω_1 is scanned over the free-bound $n' = -17$ transition for a number of different intensities of L_2. The Autler-Townes splitting of the one-photon line is clearly visible as the intensity of the bound-bound laser is increased. The Rabi frequency Ω_{BB} is extracted by fitting Eq. (1) to the data, and is approximately the splitting of the two peaks as

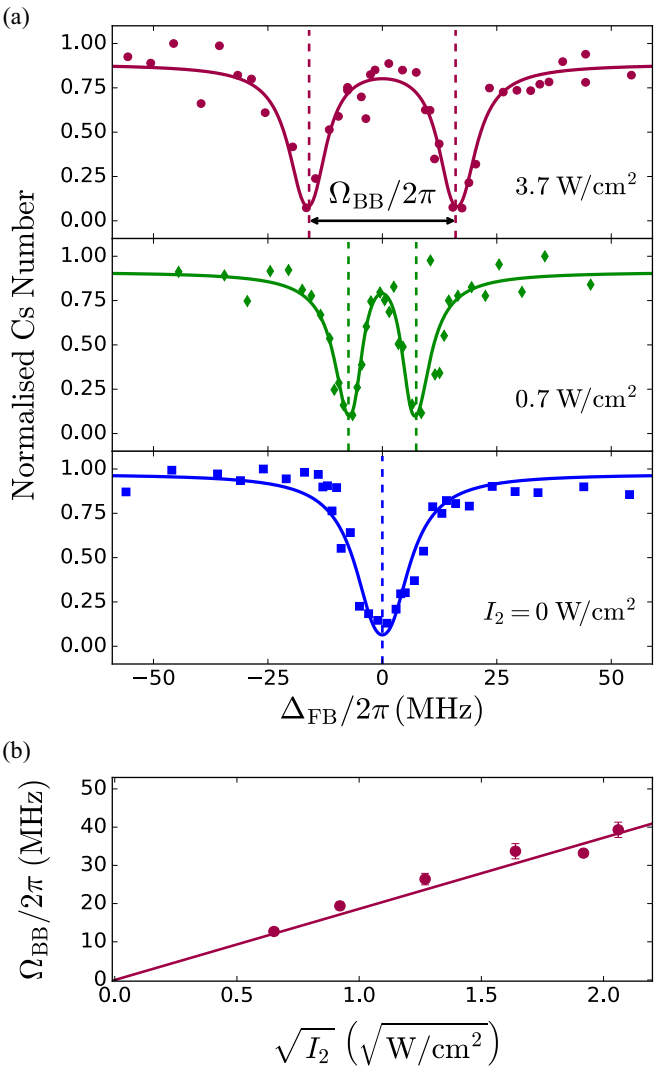

FIG. 5. Autler-Townes spectroscopy (ATS) of the $n' = -17 \rightarrow n'' = -5$ transition in $Cs^{174}Yb$. (a) Normalized Cs number vs detuning, Δ_{FB}, of laser L_1 from the $n' = -17$ free-bound transition. The second laser L_2 is on resonance with the bound-bound transition, $\Delta_{BB} = 0$, and the splitting of the one-photon line shape is observed for varying intensities I_2 of laser L_2. (b) Bound-bound Rabi frequency Ω_{BB} extracted from the ATS measurements as a function of the square root of the intensity I_2 of laser L_2 that drives the bound-bound transition. The solid line is a linear fit with the intercept constrained to be zero.

labeled in the figure. The quantity of interest, $\Omega_{BB}/\sqrt{I_2}$, is then extracted from a linear fit, as shown in Fig. 5(b). We find that for the $n' = -17 \rightarrow n'' = -5$ transition, $\Omega_{BB}/\sqrt{I_2} = 2\pi \times 19(1)$ MHz$/\sqrt{\text{W cm}^{-2}}$. We include this measurement in Fig. 4 as the red closed circle. We did not measure all the transitions using ATS due to the ∼30 s load-detection cycle associated with conducting the measurements. Nevertheless, the excellent agreement between the two measurements of the line strength for the $n' = -17 \rightarrow n'' = -5$ transition confirms the validity of using the light-shift measurements.

The FCFs that determine the line strengths are dominated by the region around the outermost lobe of the wave function for $n' = -17$. This is far inside the outer turning points of

the near-threshold levels of the ground electronic state. In this region, the wave functions of the different near-threshold levels in the electronic ground state are almost in phase with one another, but with amplitudes proportional to $E_{\rm b1}^{1/3}$ [93] and line strengths proportional to $E_{\rm b1}^{2/3}$. However, the wave functions start to change phase as $E_{\rm b1}$ increases; eventually the phase difference between the wave functions in the two electronic states overcomes the amplitude factor and the FCF starts to decrease. Figure 4 shows that the peak line strength occurs around $n'' = -5$ in the present case.

Guttridge *et al.* [77] fitted the one-photon photoassociation spectra to a near-dissociation expansion. However, the quantities C_6 and C_8 resulting from this are *effective* dispersion coefficients that incorporate higher-order effects. They are not sufficient to determine the outer turning point accurately at the energy of the $n' = -17$ level, which is bound by 286 GHz. Calculating FCFs will require a more complete model of the excited-state potential, which is beyond the scope of this paper.

IV. DETERMINATION OF THE INTERACTION POTENTIAL

The spacings between near-threshold bound states are largely determined by the long-range potential,

$$V(R) \sim \sum_{n=6,8,10,\ldots} -C_n R^{-n} \quad (\text{as } R \to \infty), \tag{3}$$

where C_n are dispersion coefficients. However, at least one additional parameter is needed to specify the actual positions of the levels. To the extent that the long-range potential is described by Eq. (3), only one such parameter is needed. This parameter may be thought of as the binding energy of the least-bound state, the scattering length, or the noninteger vibrational quantum number at dissociation. Physically, it is determined by the potential at short range and is sometimes described as the "volume" of the potential well, as quantified by the Wentzel-Kramers-Brillouin (WKB) phase integral at dissociation,

$$\Phi = \int_{R_{\rm in}}^{\infty} \sqrt{\frac{-2\mu}{\hbar^2} V(R)}\, dR, \tag{4}$$

where $R_{\rm in}$ is the inner turning point. For a single isotopolog, potentials with the same fractional part of Φ/π have the same near-threshold bound states (and the same scattering length), even if they have a different number of vibrational levels, $N_{\rm vib} = {\rm int}(\Phi/\pi + \frac{3}{8})$. The Born-Oppenheimer potential $V(R)$ is independent of reduced mass μ, but the dependence of Φ on μ means that potentials with different $N_{\rm vib}$ for one isotopolog imply different values of the fractional part of Φ/π, and hence different level positions for other isotopologs. Comparing measurements for different isotopologs can thus establish the number of vibrational levels supported by the potential.

Calculations of Feshbach resonance widths [55,58] require a complete interaction potential $V(R)$, rather than just the long-range form given by Eq. (3). To obtain such a potential, we base the short-range part on electronic structure calculations. Interaction potentials for the $^2\Sigma$ ground state of CsYb have been calculated at various levels of electronic structure theory [58,59,94,95]. The potential is dominated by dispersion interactions, with little chemical bonding, due to the large difference in ionization energies for Cs and Yb [96]. We therefore choose to base our short-range potential on that of Brue and Hutson [58], as the coupled-cluster methods and basis sets they used are likely to give a good description of the dispersion interactions.

The potential of Ref. [58] has a well depth of $hc \times 620\,{\rm cm}^{-1}$ and supports 69 vibrational levels. In order to adjust this potential to fit our measured binding energies, we first represent it in an analytic form,

$$V(R) = Ae^{-\beta R} - \sum_{n=6,8,10} D_n(\beta R) C_n R^{-n}. \tag{5}$$

Here, A and β control the magnitude and range of the short-range repulsive wall of the potential and

$$D_n(\beta R) = 1 - e^{-\beta R} \sum_{m=0}^{n} \frac{(\beta R)^m}{m!} \tag{6}$$

is a Tang-Toennies damping function [97]. To reduce the number of free parameters, we use $C_{10} = (49/40)C_8^2/C_6$ as recommended by Thakkar and Smith [98]. We fit the parameters A, β, C_6, and C_8 to the interaction energies from the electronic structure calculations of Ref. [58]. The functional form accurately represents the *ab initio* points, and the fit is not significantly improved by including an attractive exponential term; this confirms that there is little chemical bonding. The value of C_6 obtained in this way is 3800 $E_{\rm h}a_0^6$, which is about 13% larger than the value of 3370 $E_{\rm h}a_0^6$ obtained in Ref. [58] using Tang's combination rule [99]. Here, a_0 is the Bohr radius and $E_{\rm h}$ is the Hartree energy. This confirms that the electronic structure calculations of Ref. [58] are adequate to give a qualitative (but not quantitative) description of the dispersion effects.

To fit the potential to the measured binding energies, we fit the dispersion coefficients C_6 and C_8, and vary A to adjust the volume of the potential and thus the number of vibrational levels. We fix $\beta = 0.83\,a_0^{-1}$ to the value obtained from fitting to the electronic structure calculations. These choices allow us to fit the aspects of the potential that are well determined by our measurements, using a small number of parameters, while maintaining a physically reasonable form for the entire potential.

We calculate near-threshold bound states supported by the potential using the BOUND package [101]. The terms in the Hamiltonian that couple different electronic and nuclear spin channels (and cause Feshbach resonances) are very small [58]. The effective potential is thus almost identical for all spin channels. The bound molecular states are almost unaffected by these weak couplings. The effects of the atomic hyperfine splitting and Zeeman shifts are already accounted for in the measurement of the binding energies. We therefore calculate bound states using single-channel calculations, neglecting electron and nuclear spins and the effects of the magnetic field.

We carry out separate least-squares fits to the measured binding energies for each plausible number of vibrational levels, $N_{\rm vib}$ [102]. We fit to all three isotopologs simultaneously, using weights derived from the experimental uncertainties. We find the best fit for $N_{\rm vib} = 77$ with a reduced chi-squared $\chi_\nu^2 = 1.3$. For $N_{\rm vib} = 76$ and 78, we find $\chi_\nu^2 = 25$ and 26,

TABLE II. Fitted parameters and statistical uncertainties (1σ) from the least-squares fit to the binding energies. The sensitivity is as defined in Ref. [100].

Parameter	Value	Uncertainty	Sensitivity
A/E_h	13.8866515	0.2	2×10^{-7}
$C_6/E_h a_0^6$	3463.2060	4	2×10^{-4}
$C_8/E_h a_0^8$	502560.625	5000	5×10^{-3}

respectively. The final fitted parameters are given in Table II, with their uncertainties and sensitivities [100]. As this is a very strongly correlated fit, rounding the fitted parameters to their uncertainties introduces very large errors in the calculated levels, so the parameters are given to a number of significant figures determined by their sensitivity [100] to allow accurate reproduction of the binding energies. The fitted value of C_6 is within 3% of the value from Tang's combining rule [58]. The ground-state binding energies calculated from the fitted interaction potential are included in Table I.

The statistical uncertainties in the potential parameters are very small. However, our model is somewhat restrictive, and the uncertainties in quantities derived from the potential are dominated by model dependence. To quantify this, we have explored a range of different models; these include using different values of β and adding an attractive exponential term in the fit to the electronic structure calculations. The estimates of uncertainties due to model dependence given below are based on the variations observed in these tests. Further measurements of more deeply bound vibrational states would be necessary to determine the details of the short-range potential.

Figure 6 shows the final fitted potential, along with the unmodified potential of Brue and Hutson [58]. The well depths D_e and equilibrium distances R_e for the ground-state potentials from Refs. [94], [58], [59], and [95] are compared with those

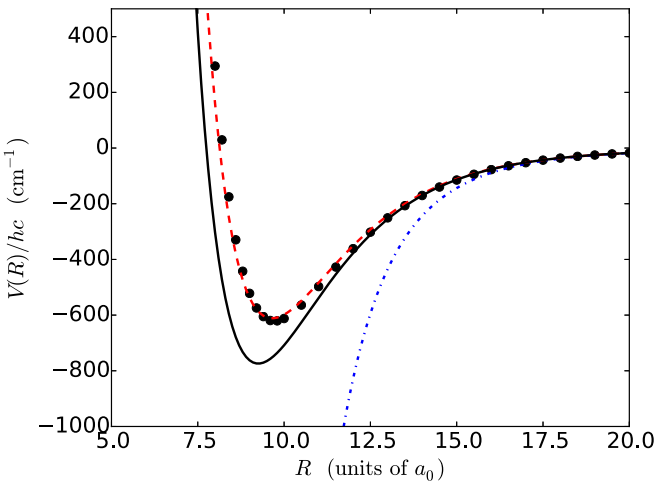

FIG. 6. Potential curves for the $X\,^2\Sigma^+_{1/2}$ ground state of CsYb. The dots are the electronic structure calculations of Ref. [58]; the red dashed line is the functional form given by Eq. (5) fitted to the electronic structure calculations; the solid black line is the final fitted potential; and the blue dash-dotted line is the pure dispersion potential, given by Eq. (3), without a repulsive wall or dispersion damping functions.

TABLE III. Comparison of well depths and equilibrium distances of CsYb potentials. The uncertainties for the potential of the present work are dominated by model dependence, not statistics.

Ref.	D_e/hc (cm^{-1})	R_e (units of a_0)
This work	770(30)	9.25(50)
[94]	182	10.69
[58]	621	9.72
[59]	159	10.89
[95]	542	9.75

for our fitted potential in Table III. The minimum of our potential is deeper and at shorter range than any of those from electronic structure calculations, though comparable to those from Refs. [58] and [95]. There is an inverse correlation between D_e and R_e for the different potentials from electronic structure calculations. References [94] and [59] both used large-core effective core potentials for Yb, with only two active electrons; this might be responsible for their large equilibrium distances and small well depths, which are in poor agreement with the experimental results.

V. PREDICTION OF SCATTERING LENGTHS

We have used our fitted potential to predict interspecies scattering lengths for all isotope combinations of Cs+Yb. These are given in Table IV. In this case, the uncertainties from statistics and model dependence are comparable, though the latter are larger. The scattering lengths are also shown as a function of reduced mass in Fig. 7, along with both observed and calculated binding energies. The cube root of the binding energy varies almost linearly with reduced mass for an interaction potential with $-C_6/R^6$ long-range behavior [93], except for a small curvature very near dissociation due to the Gribakin-Flambaum correction [103] of $\pi/8$ to the WKB quantization condition at threshold.

The scattering lengths are in remarkably good agreement with our previous estimates based on interspecies thermalization [39]. Six of the isotope combinations have scattering lengths between $-2\bar{a}$ and $2\bar{a}$, where $\bar{a}$ is the mean scattering length of Gribakin and Flambaum [103]. The exception is Cs+^{176}Yb, which has a very large scattering length due to

TABLE IV. Interspecies scattering lengths calculated from the fitted interaction potential. Both statistical uncertainties (1σ) and estimated uncertainties from model dependence are given.

Mixture	a (units of a_0)	Statistical uncertainty (units of a_0)	Model dependence (units of a_0)
Cs+^{168}Yb	165.98	0.15	0.4
Cs+^{170}Yb	96.24	0.08	0.2
Cs+^{171}Yb	69.99	0.08	0.3
Cs+^{172}Yb	41.03	0.12	0.5
Cs+^{173}Yb	1.0	0.2	1.0
Cs+^{174}Yb	−74.8	0.5	3
Cs+^{176}Yb	798	7	40

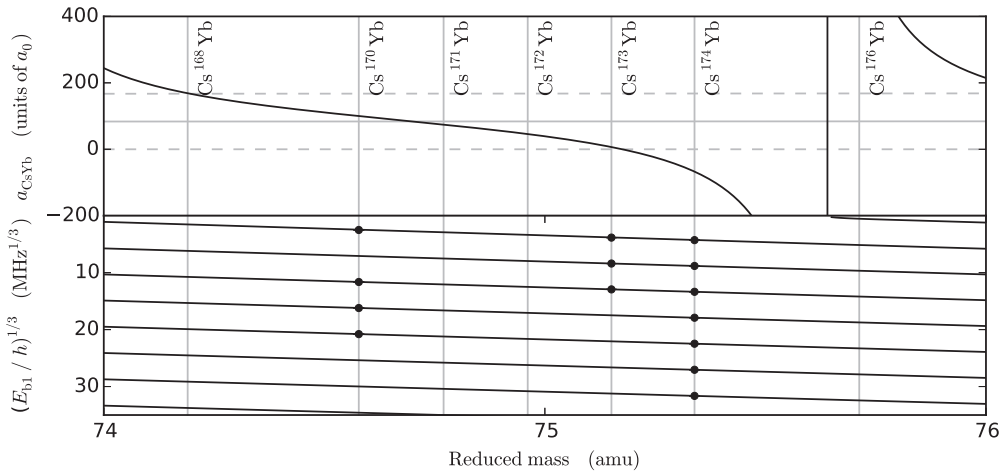

FIG. 7. Interspecies scattering length (upper panel) and binding energies (lower panel) for CsYb as a function of reduced mass, calculated using the fitted interaction potential. Points show measured levels; error bars are smaller than the points on this scale. The vertical lines correspond to the stable Yb isotopes. The horizontal lines on the upper figure correspond to $a = 0, \bar{a}$, and $2\bar{a}$.

the presence of an additional vibrational level just below threshold. The moderate values of the scattering length for four of the bosonic Yb isotopes should allow the production of miscible two-species condensates [104] with Cs at the magnetic field required to minimize the Cs three-body loss rate [105]. Conversely, the large positive scattering length for Cs+^{176}Yb is likely to result in an enhancement of the widths of Feshbach resonances [58]. The negative interspecies scattering length for Cs+^{174}Yb opens up the intriguing prospect of forming self-bound quantum droplets [106–108]. The very small interspecies scattering length of Cs+^{173}Yb indicates that the degenerate Bose-Fermi mixture would be essentially noninteracting. In contrast, the scattering length of 70 a_0 for Cs+^{171}Yb is ideal for sympathetic cooling of ^{171}Yb to degeneracy [28,38], overcoming the problem of the small intraspecies scattering length [69] that makes direct evaporative cooling ineffective.

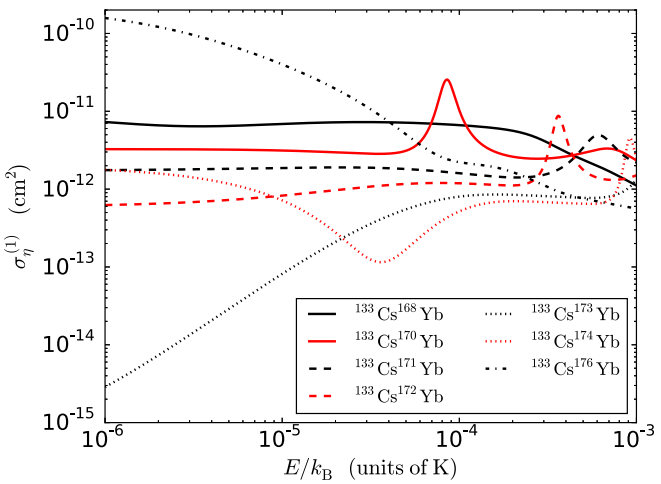

FIG. 8. Calculated cross sections for interspecies thermalization of Cs with Yb, as a function of collision energy E.

Figure 8 shows the cross sections $\sigma_\eta^{(1)}$ that characterize interspecies thermalization [109], as a function of collision energy, for all the isotope combinations. These are obtained from single-channel quantum scattering calculations on the fitted interaction potential, using the MOLSCAT package [110] and the postprocessor SBE [111], including all relevant partial waves. The low-energy cross sections vary across more than four orders of magnitude. Cs+^{173}Yb has a very small cross section at low energy, due to its tiny zero-energy scattering length, but this increases rapidly with energy due to both effective-range effects and p-wave scattering. Cs+^{174}Yb has a negative scattering length at zero energy, and the cross section exhibits a Ramsauer-Townsend minimum near 30 μK, where the energy-dependent scattering length crosses zero. However, the minimum is not particularly deep because 30 μK is high enough that the p-wave contributions are significant. Cs+^{170}Yb exhibits a d-wave shape resonance around 90 μK, while Cs+^{171}Yb and Cs+^{172}Yb exhibit f-wave shape resonances around 600 and 400 μK, respectively. Cs+^{173}Yb and Cs+^{174}Yb exhibit g-wave shape resonances at even higher energies.

VI. CONCLUSION

We have used two-photon photoassociation spectroscopy to measure the binding energies of vibrational levels of the electronic ground state of the heteronuclear CsYb molecule. We measure the binding energy of vibrational levels for three isotopologs of CsYb. This is sufficient to establish that the ground state supports 77 vibrational levels. We fit a ground-state interaction potential based on electronic structure calculations to the binding energies for all the isotopologs together. Using our optimized potential, we calculate values of the s-wave scattering length for all seven isotopic combinations of ^{133}Cs and Yb. The results are very promising for the sympathetic cooling of ^{171}Yb and for the production of quantum-degenerate mixtures.

The fitted interaction potential may be used to predict positions and widths of interspecies Feshbach resonances [55,57,58]. Magnetoassociation using these predicted Fesh-

bach resonances, followed by STIRAP [112], is a promising route to the creation of ultracold ground-state $^2\Sigma$ molecules.

The data presented in this work are available from Durham University [113].

ACKNOWLEDGMENTS

We acknowledge support from the UK Engineering and Physical Sciences Research Council (Grants No. EP/N007085/1, No. EP/P008275/1, and No. EP/P01058X/1).

[1] K. Mølmer, Phys. Rev. Lett. **80**, 1804 (1998).
[2] M. Lewenstein, L. Santos, M. A. Baranov, and H. Fehrmann, Phys. Rev. Lett. **92**, 050401 (2004).
[3] M. Zaccanti, C. D'Errico, F. Ferlaino, G. Roati, M. Inguscio, and G. Modugno, Phys. Rev. A **74**, 041605 (2006).
[4] S. Ospelkaus, C. Ospelkaus, L. Humbert, K. Sengstock, and K. Bongs, Phys. Rev. Lett. **97**, 120403 (2006).
[5] K. Günter, T. Stöferle, H. Moritz, M. Köhl, and T. Esslinger, Phys. Rev. Lett. **96**, 180402 (2006).
[6] K. Sengupta, N. Dupuis, and P. Majumdar, Phys. Rev. A **75**, 063625 (2007).
[7] F. M. Marchetti, C. J. M. Mathy, D. A. Huse, and M. M. Parish, Phys. Rev. B **78**, 134517 (2008).
[8] S.-K. Tung, K. Jiménez-García, J. Johansen, C. V. Parker, and C. Chin, Phys. Rev. Lett. **113**, 240402 (2014).
[9] R. Pires, J. Ulmanis, S. Häfner, M. Repp, A. Arias, E. D. Kuhnle, and M. Weidemüller, Phys. Rev. Lett. **112**, 250404 (2014).
[10] R. A. W. Maier, M. Eisele, E. Tiemann, and C. Zimmermann, Phys. Rev. Lett. **115**, 043201 (2015).
[11] J. Ulmanis, S. Häfner, R. Pires, E. D. Kuhnle, Y. Wang, C. H. Greene, and M. Weidemüller, Phys. Rev. Lett. **117**, 153201 (2016).
[12] T. Köhler, K. Góral, and P. S. Julienne, Rev. Mod. Phys. **78**, 1311 (2006).
[13] K.-K. Ni, S. Ospelkaus, M. H. G. de Miranda, A. Pe'er, B. Neyenhuis, J. J. Zirbel, S. Kotochigova, P. S. Julienne, D. S. Jin, and J. Ye, Science **322**, 231 (2008).
[14] F. Lang, K. Winkler, C. Strauss, R. Grimm, and J. Hecker Denschlag, Phys. Rev. Lett. **101**, 133005 (2008).
[15] K. Aikawa, D. Akamatsu, J. Kobayashi, M. Ueda, T. Kishimoto, and S. Inouye, New J. Phys. **11**, 055035 (2009).
[16] M. P. Köppinger, D. J. McCarron, D. L. Jenkin, P. K. Molony, H.-W. Cho, S. L. Cornish, C. R. Le Sueur, C. L. Blackley, and J. M. Hutson, Phys. Rev. A **89**, 033604 (2014).
[17] P. K. Molony, P. D. Gregory, Z. Ji, B. Lu, M. P. Köppinger, C. R. Le Sueur, C. L. Blackley, J. M. Hutson, and S. L. Cornish, Phys. Rev. Lett. **113**, 255301 (2014).
[18] P. K. Molony, A. Kumar, P. D. Gregory, R. Kliese, T. Puppe, C. R. Le Sueur, J. Aldegunde, J. M. Hutson, and S. L. Cornish, Phys. Rev. A **94**, 022507 (2016).
[19] T. Takekoshi, L. Reichsöllner, A. Schindewolf, J. M. Hutson, C. R. Le Sueur, O. Dulieu, F. Ferlaino, R. Grimm, and H.-C. Nägerl, Phys. Rev. Lett. **113**, 205301 (2014).
[20] J. W. Park, S. A. Will, and M. W. Zwierlein, Phys. Rev. Lett. **114**, 205302 (2015).
[21] M. Guo, B. Zhu, B. Lu, X. Ye, F. Wang, R. Vexiau, N. Bouloufa-Maafa, G. Quéméner, O. Dulieu, and D. Wang, Phys. Rev. Lett. **116**, 205303 (2016).
[22] J. L. Bohn, A. M. Rey, and J. Ye, Science **357**, 1002 (2017).
[23] G. Modugno, G. Ferrari, G. Roati, R. J. Brecha, A. Simoni, and M. Inguscio, Science **294**, 1320 (2001).
[24] M. Mudrich, S. Kraft, K. Singer, R. Grimm, A. Mosk, and M. Weidemüller, Phys. Rev. Lett. **88**, 253001 (2002).
[25] Z. Hadzibabic, C. A. Stan, K. Dieckmann, S. Gupta, M. W. Zwierlein, A. Görlitz, and W. Ketterle, Phys. Rev. Lett. **88**, 160401 (2002).
[26] M. Taglieber, A.-C. Voigt, T. Aoki, T. W. Hänsch, and K. Dieckmann, Phys. Rev. Lett. **100**, 010401 (2008).
[27] F. M. Spiegelhalder, A. Trenkwalder, D. Naik, G. Hendl, F. Schreck, and R. Grimm, Phys. Rev. Lett. **103**, 223203 (2009).
[28] S. Taie, Y. Takasu, S. Sugawa, R. Yamazaki, T. Tsujimoto, R. Murakami, and Y. Takahashi, Phys. Rev. Lett. **105**, 190401 (2010).
[29] H. W. Cho, D. J. McCarron, D. L. Jenkin, M. P. Köppinger, and S. L. Cornish, Eur. Phys. J. D **65**, 125 (2011).
[30] D. J. McCarron, H. W. Cho, D. L. Jenkin, M. P. Köppinger, and S. L. Cornish, Phys. Rev. A **84**, 011603 (2011).
[31] A. Ridinger, S. Chaudhuri, T. Salez, U. Eismann, D. R. Fernandes, K. Magalhães, D. Wilkowski, C. Salomon, and F. Chevy, Eur. Phys. J. D **65**, 223 (2011).
[32] L. Wacker, N. B. Jørgensen, D. Birkmose, R. Horchani, W. Ertmer, C. Klempt, N. Winter, J. Sherson, and J. J. Arlt, Phys. Rev. A **92**, 053602 (2015).
[33] M. Gröbner, P. Weinmann, F. Meinert, K. Lauber, E. Kirilov, and H.-C. Nägerl, J. Mod. Opt. **63**, 1829 (2016).
[34] S. Tassy, N. Nemitz, F. Baumer, C. Höhl, A. Batär, and A. Görlitz, J. Phys. B **43**, 205309 (2010).
[35] H. Hara, H. Konishi, S. Nakajima, Y. Takasu, and Y. Takahashi, J. Phys. Soc. Jpn. **83**, 014003 (2014).
[36] B. Pasquiou, A. Bayerle, S. M. Tzanova, S. Stellmer, J. Szczepkowski, M. Parigger, R. Grimm, and F. Schreck, Phys. Rev. A **88**, 023601 (2013).
[37] A. Khramov, A. Hansen, W. Dowd, R. J. Roy, C. Makrides, A. Petrov, S. Kotochigova, and S. Gupta, Phys. Rev. Lett. **112**, 033201 (2014).
[38] V. D. Vaidya, J. Tiamsuphat, S. L. Rolston, and J. V. Porto, Phys. Rev. A **92**, 043604 (2015).
[39] A. Guttridge, S. A. Hopkins, S. L. Kemp, M. D. Frye, J. M. Hutson, and S. L. Cornish, Phys. Rev. A **96**, 012704 (2017).
[40] A. S. Flores, H. P. Mishra, W. Vassen, and S. Knoop, Eur. Phys. J. D **71**, 49 (2017).
[41] M. Witkowski, B. Nagórny, R. Munoz-Rodriguez, R. Ciuryło, P. S. Żuchowski, S. Bilicki, M. Piotrowski, P. Morzyński, and M. Zawada, Opt. Express **25**, 3165 (2017).
[42] A. Micheli, G. Brennen, and P. Zoller, Nat. Phys. **2**, 341 (2006).
[43] J. Pérez-Ríos, F. Herrera, and R. V. Krems, New J. Phys. **12**, 103007 (2010).
[44] F. Herrera, Y. Cao, S. Kais, and K. B. Whaley, New J. Phys. **16**, 075001 (2014).
[45] S. V. Alyabyshev, M. Lemeshko, and R. V. Krems, Phys. Rev. A **86**, 013409 (2012).
[46] T. A. Isaev, S. Hoekstra, and R. Berger, Phys. Rev. A **82**, 052521 (2010).

[47] V. V. Flambaum and M. G. Kozlov, Phys. Rev. Lett. **99**, 150801 (2007).

[48] J. J. Hudson, D. M. Kara, I. J. Smallman, B. E. Sauer, M. R. Tarbutt, and E. A. Hinds, Nature (London) **473**, 493 (2011).

[49] E. Abrahamsson, T. V. Tscherbul, and R. V. Krems, J. Chem. Phys. **127**, 044302 (2007).

[50] G. Quéméner and J. L. Bohn, Phys. Rev. A **93**, 012704 (2016).

[51] S. A. Hopkins, K. Butler, A. Guttridge, S. Kemp, R. Freytag, E. A. Hinds, M. R. Tarbutt, and S. L. Cornish, Rev. Sci. Instrum. **87**, 043109 (2016).

[52] S. L. Kemp, K. L. Butler, R. Freytag, S. A. Hopkins, E. A. Hinds, M. R. Tarbutt, and S. L. Cornish, Rev. Sci. Instrum. **87**, 023105 (2016).

[53] A. Guttridge, S. A. Hopkins, S. L. Kemp, D. Boddy, R. Freytag, M. P. A. Jones, M. R. Tarbutt, E. A. Hinds, and S. L. Cornish, J. Phys. B **49**, 145006 (2016).

[54] C. Chin, R. Grimm, P. Julienne, and E. Tiesinga, Rev. Mod. Phys. **82**, 1225 (2010).

[55] P. S. Żuchowski, J. Aldegunde, and J. M. Hutson, Phys. Rev. Lett. **105**, 153201 (2010).

[56] D. A. Brue and J. M. Hutson, Phys. Rev. Lett. **108**, 043201 (2012).

[57] V. Barbé, A. Ciamei, B. Pasquiou, L. Reichsöllner, F. Schreck, P. S. Żuchowski, and J. M. Hutson, Nat. Phys. (2018), doi: 10.1038/s41567-018-0169-x.

[58] D. A. Brue and J. M. Hutson, Phys. Rev. A **87**, 052709 (2013).

[59] D. N. Meniailava and M. B. Shundalau, Comput. Theor. Chem. **1111**, 20 (2017).

[60] J. L. Bohn and P. S. Julienne, Phys. Rev. A **60**, 414 (1999).

[61] K. M. Jones, E. Tiesinga, P. D. Lett, and P. S. Julienne, Rev. Mod. Phys. **78**, 483 (2006).

[62] E. R. I. Abraham, W. I. McAlexander, J. M. Gerton, R. G. Hulet, R. Côté, and A. Dalgarno, Phys. Rev. A **53**, R3713 (1996).

[63] C. C. Tsai, R. S. Freeland, J. M. Vogels, H. M. J. M. Boesten, B. J. Verhaar, and D. J. Heinzen, Phys. Rev. Lett. **79**, 1245 (1997).

[64] F. A. van Abeelen and B. J. Verhaar, Phys. Rev. A **59**, 578 (1999).

[65] H. Wang, A. N. Nikolov, J. R. Ensher, P. L. Gould, E. E. Eyler, W. C. Stwalley, J. P. Burke, Jr., J. L. Bohn, C. H. Greene, E. Tiesinga, C. J. Williams, and P. S. Julienne, Phys. Rev. A **62**, 052704 (2000).

[66] N. Vanhaecke, C. Lisdat, B. T'Jampens, D. Comparat, A. Crubellier, and P. Pillet, Eur. Phys. J. D **28**, 351 (2004).

[67] S. Moal, M. Portier, J. Kim, J. Dugué, U. D. Rapol, M. Leduc, and C. Cohen-Tannoudji, Phys. Rev. Lett. **96**, 023203 (2006).

[68] Y. N. Martinez de Escobar, P. G. Mickelson, P. Pellegrini, S. B. Nagel, A. Traverso, M. Yan, R. Côté, and T. C. Killian, Phys. Rev. A **78**, 062708 (2008).

[69] M. Kitagawa, K. Enomoto, K. Kasa, Y. Takahashi, R. Ciuryło, P. Naidon, and P. S. Julienne, Phys. Rev. A **77**, 012719 (2008).

[70] W. Gunton, M. Semczuk, N. S. Dattani, and K. W. Madison, Phys. Rev. A **88**, 062510 (2013).

[71] E. Pachomow, V. P. Dahlke, E. Tiemann, F. Riehle, and U. Sterr, Phys. Rev. A **95**, 043422 (2017).

[72] F. Münchow, C. Bruni, M. Madalinski, and A. Gorlitz, Phys. Chem. Chem. Phys. **13**, 18734 (2011).

[73] M. Debatin, T. Takekoshi, R. Rameshan, L. Reichsöllner, F. Ferlaino, R. Grimm, R. Vexiau, N. Bouloufa, O. Dulieu, and H.-C. Nägerl, Phys. Chem. Chem. Phys. **13**, 18926 (2011).

[74] M. Guo, R. Vexiau, B. Zhu, B. Lu, N. Bouloufa-Maafa, O. Dulieu, and D. Wang, Phys. Rev. A **96**, 052505 (2017).

[75] S. Dutta, J. Pérez-Ríos, D. S. Elliott, and Y. P. Chen, Phys. Rev. A **95**, 013405 (2017).

[76] T. M. Rvachov, H. Son, J. J. Park, S. Ebadi, M. W. Zwierlein, W. Ketterle, and A. O. Jamison, Phys. Chem. Chem. Phys. **20**, 4739 (2018).

[77] A. Guttridge, S. A. Hopkins, M. D. Frye, J. J. McFerran, J. M. Hutson, and S. L. Cornish, Phys. Rev. A **97**, 063414 (2018).

[78] R. W. P. Drever, J. L. Hall, F. V. Kowalski, J. Hough, G. M. Ford, A. J. Munley, and H. Ward, Appl. Phys. B **31**, 97 (1983).

[79] J. I. Thorpe, K. Numata, and J. Livas, Opt. Express **16**, 15980 (2008).

[80] P. D. Gregory, P. K. Molony, M. P. Köppinger, A. Kumar, Z. Ji, B. Lu, A. L. Marchant, and S. L. Cornish, New J. Phys. **17**, 055006 (2015).

[81] K. Winkler, G. Thalhammer, M. Theis, H. Ritsch, R. Grimm, and J. H. Denschlag, Phys. Rev. Lett. **95**, 063202 (2005).

[82] M. Fleischhauer, A. Imamoglu, and J. P. Marangos, Rev. Mod. Phys. **77**, 633 (2005).

[83] The production of Cs*Yb molecules causes a detectable loss of Cs atoms from the trap.

[84] J. L. Bohn and P. S. Julienne, Phys. Rev. A **54**, R4637 (1996).

[85] M. Portier, M. Leduc, and C. Cohen-Tannoudji, Faraday Discuss. **142**, 415 (2009).

[86] U. Fano, Phys. Rev. **124**, 1866 (1961).

[87] R. G. Brewer and E. L. Hahn, Phys. Rev. A **11**, 1641 (1975).

[88] G. Orriols, Nuovo Cimento B **53**, 1 (1979).

[89] B. Lounis and C. Cohen-Tannoudji, J. Phys. **2**, 579 (1992).

[90] T. Zanon-Willette, E. de Clercq, and E. Arimondo, Phys. Rev. A **84**, 062502 (2011).

[91] C. Cohen-Tannoudji, Phys. Scr. **90**, 088013 (2015).

[92] The definition of Ω_{BB} in Eq. (2) is twice that in Ref. [85] .

[93] R. J. Le Roy and R. B. Bernstein, J. Chem. Phys. **52**, 3869 (1970).

[94] E. R. Meyer and J. L. Bohn, Phys. Rev. A **80**, 042508 (2009).

[95] Q. Shao, L. Deng, X. Xing, D. Gou, X. Kuang, and H. Li, J. Phys. Chem. A **121**, 2187 (2017).

[96] These ionization energies are 3.9 eV for Cs and 6.3 eV for Yb.

[97] K. T. Tang and J. P. Toennies, J. Chem. Phys. **80**, 3726 (1984).

[98] A. J. Thakkar and V. H. Smith, J. Phys. B **7**, L321 (1974).

[99] K. T. Tang, Phys. Rev. **177**, 108 (1969).

[100] R. J. Le Roy, J. Mol. Spectrosc. **191**, 223 (1998).

[101] J. M. Hutson, computer code BOUND, version 5 (Collaborative Computational Project No. 6 of the UK Engineering and Physical Sciences Research Council, UK, 1993).

[102] In principle, the potential might support different numbers of vibrational levels for different isotopologs, but we find that the three isotopologs for which we have measurements have the same number of vibrational levels.

[103] G. F. Gribakin and V. V. Flambaum, Phys. Rev. A **48**, 546 (1993).

[104] F. Riboli and M. Modugno, Phys. Rev. A **65**, 063614 (2002).

[105] T. Weber, J. Herbig, M. Mark, H.-C. Nägerl, and R. Grimm, Phys. Rev. Lett. **91**, 123201 (2003).

[106] D. S. Petrov, Phys. Rev. Lett. **115**, 155302 (2015).
[107] C. R. Cabrera, L. Tanzi, J. Sanz, B. Naylor, P. Thomas, P. Cheiney, and L. Tarruell, Science **359**, 301 (2018).
[108] P. Cheiney, C. R. Cabrera, J. Sanz, B. Naylor, L. Tanzi, and L. Tarruell, Phys. Rev. Lett. **120**, 135301 (2018).
[109] M. D. Frye and J. M. Hutson, Phys. Rev. A **89**, 052705 (2014).
[110] J. M. Hutson and S. Green, computer code MOLSCAT, version 14 (Collaborative Computational Project No. 6 of the UK Engineering and Physical Sciences Research Council, UK, 1994).
[111] J. M. Hutson and S. Green, computer code SBE (Collaborative Computational Project No. 6 of the UK Engineering and Physical Sciences Research Council, UK, 1982).
[112] K. Bergmann, H. Theuer, and B. Shore, Rev. Mod. Phys. **70**, 1003 (1998).
[113] http://dx.doi.org/10.15128/r1qz20ss50n.